

REDUCING SKIN FRICTION AND HEAT TRANSFER OVER A HYPERSONIC CRUISING
VEHICLE BY MASS INJECTION

By

YOSHIFUMI NOZAKI

A THESIS PRESENTED TO THE GRADUATE SCHOOL
OF THE UNIVERSITY OF FLORIDA IN PARTIAL FULFILLMENT
OF THE REQUIREMENTS FOR THE DEGREE OF
MASTER OF SCIENCE

UNIVERSITY OF FLORIDA

2007

©2007 Yoshifumi Nozaki

To my parents, Yoshikazu Nozaki and Keiko Nozaki, and my brother, Toshihiro Nozaki. You have inspired me to become who I am today. Thank you for always supporting and believing in me. I dedicate this to you.

ACKNOWLEDGMENTS

I gratefully acknowledge the support provided by Dr. Pasquale M. Sforza, Professor of Mechanical and Aerospace Engineering at the University of Florida.

TABLE OF CONTENTS

	<u>page</u>
ACKNOWLEDGMENTS	4
LIST OF TABLES	7
LIST OF FIGURES	8
ABSTRACT	16
CHAPTER	
1 INVISCID ANALYSIS	17
Introduction.....	17
Local Surface Inclination Method	17
Inviscid Aerodynamic Forces and Moments	19
2 VISCOUS AND HIGH TEMPERATURE CONSIDERATIONS	22
Introduction.....	22
Local Reynolds Number	22
Local Skin Friction	26
Local Heat Transfer	28
Total Forces Acting on the Vehicle.....	31
Discussion of Results without any Cooling Methods.....	32
3 MASS INJECTION EFFECTS	42
Introduction.....	42
Effects of Mass Injection on the Boundary Layer	43
General Behavior of Reducing Skin Friction and Heating.....	44
4 RESULTS	47
Introduction.....	47
The Range Equation	47
Comparison of Range, L /D, and Heat Transfer Variance	49
5 CONCLUSIONS	95
Conclusions of this Study	95
Future Work.....	96
APPENDIX	
A MATLAB CODE TO COMPUTE FLIGHT PERFORMANCE OF X24C.....	98

B	MATLAB CODE (FUNCTION) TO COMPUTE TEMPERATURE	129
C	MATLAB CODE (FUNCTION) TO COMPUTE DENSITY	132
D	MATLAB CODE (FUNCTION) TO COMPUTE VOSCOSITY	134
E	MATLAB CODE (FUNCTION) TO COMPUTE PRANDTL NUMBER.....	136
F	MATLAB CODE (FUNCTION) TO COMPUTE ENTHALPY	138
G	MATLAB CODE (FUNCTION) TO COMPUTE MACH NUMBER FOR PRANDTL- MAYER EXPANSION	141
	LIST OF REFERENCES	142
	BIOGRAPHICAL SKETCH	143

LIST OF TABLES

<u>Table</u>	<u>page</u>
2-1. Coefficients in Eq.(2-18)	36
2-2. Comparison of aerodynamic forces and L/D	36
2-3. Configuration of X24C studied.....	36
2-4. The effect of the base pressure on aerodynamic forces and L/D	36
4-1. Comparison of flight parameters at $M = 6$ and $30000m$ altitude. The panels that have $q_{c,w}$ of more than $50000 W/m^2$ are cooled by the mass injection rate: 0, 0.001, 0.01 (kg/m^2s).	57

LIST OF FIGURES

<u>Figure</u>	<u>page</u>
1-1. General body surface panel showing the unit normal vector along with the locations of the four corner points.....	21
2-1. Expansion wave.....	37
2-2. Deflection angle θ at the corner.....	37
2-3. Schematic diagram of stagnation region.....	37
2-4. X-24C configuration. Note that this is a representation of the right half of the aircraft.....	38
2-5. X-24C's L/D as a function of angle of attack.....	38
2-6. X-24C's aerodynamic force coefficients as a function of angle of attack.....	39
2-7. X-24C's pitching moment coefficients as a function of angle of attack.....	39
2-8. Heating distribution along windward symmetry plane of Space Shuttle Orbiter at 34.8° of angle of attack, $M = 9.15$, and $47.7km$ altitude.....	40
2-9. Comparison of surface pressure distributions around the X-24C fuselage at the farthest downstream station.....	40
2-10. Comparison of heat transfer around the X-24C fuselage at the farthest downstream station.....	41
2-11. Comparison of streamwise surface pressure distribution along the windward and leeward symmetry lines of the X-24C.....	41
3-1. Effects of mass injection on L/D with different angle of attack for a flat plate ($6m \times 6m$ square plate) at a Mach number of 6.....	45
3-2. Effects of mass injection on heat transfer with angle of attack for a flat plate ($6m \times 6m$ square plate) at a Mach number of 6.....	46
4-1. Distribution of panel area with a given heat transfer, $q_{c,w} (W/m^2)$ at $M = 6$ and $30000m$ altitude.....	57
4-2. Distribution of the number of panels with a given heat transfer, $q_{c,w} (W/m^2)$ at $M = 6$ and $30000m$ altitude.....	58

4-3.	Mass injection effect on the flight time at $M = 6$ and $30000m$ altitude. The panels to be cooled are determined by $q_{c,w} (W/m^2)$	58
4-4.	Mass injection effect on L/D at $M = 6$ and $30000m$ altitude. The panels to be cooled are determined by $q_{c,w} (W/m^2)$	59
4-5.	Mass injection effect on reduction of heat power at $M = 6$ and $30000m$ altitude. The panels to be cooled are determined by $q_{c,w} (W/m^2)$	59
4-6.	Normalized reduction of heat power v.s. normalized injected mass at $M = 6$ and $30000m$ altitude with $0.001 kg/m^2 s$ of mass injection. The panels to be cooled are determined by $q_{c,w} (W/m^2)$	60
4-7.	Flight time v.s. normalized injected mass at at $M = 6$ and $30000m$ altitude with $0.001 kg/m^2 s$ of mass injection. The panels to be cooled are determined by $q_{c,w} (W/m^2)$	60
4-8.	Flight time v.s. normalized reduction of heat power at $M = 6$ and $30000m$ altitude with $0.001 kg/m^2 s$ of mass injection. The panels to be cooled are determined by $q_{c,w} (W/m^2)$	61
4-9.	Reduction of heat power (kW) v.s. injected mass rate (kg/s) at $M = 6$ and $30000m$ altitude with $0.001 kg/m^2 s$ of mass injection. The panels to be cooled are determined by $q_{c,w} (W/m^2)$	61
4-10.	Reduction of heat energy (kJ) v.s. injected mass (kg) at $M = 6$ and $30000m$ altitude with $0.001 kg/m^2 s$ of mass injection. The panels to be cooled are determined by $q_{c,w} (W/m^2)$	62
4-11.	Flight time v.s. reduction of heat energy (kJ) at $M = 6$ and $30000m$ altitude with $0.001 kg/m^2 s$ of mass injection. The panels to be cooled are determined by $q_{c,w} (W/m^2)$	62
4-12.	Normalized reduction of heat power v.s. normalized injected mass at $M = 6$ and $30000m$ altitude with $0.01 kg/m^2 s$ of mass injection. The panels to be cooled are determined by $q_{c,w} (W/m^2)$	63
4-13.	Flight time v.s. normalized injected mass at at $M = 6$ and $30000m$ altitude with $0.01 kg/m^2 s$ of mass injection. The panels to be cooled are determined by $q_{c,w} (W/m^2)$	63

4-14.	Flight time v.s. normalized reduction of heat power at $M = 6$ and $30000m$ altitude with $0.01 \text{ kg} / \text{m}^2 \text{ s}$ of mass injection. The panels to be cooled are determined by $q_{c,w} (W / \text{m}^2)$	64
4-15.	Reduction of heat power (kW) v.s. injected mass rate (kg / s) at $M = 6$ and $30000m$ altitude with $0.01 \text{ kg} / \text{m}^2 \text{ s}$ of mass injection. The panels to be cooled are determined by $q_{c,w} (W / \text{m}^2)$	64
4-16.	Reduction of heat energy (kJ) v.s. injected mass (kg) at $M = 6$ and $30000m$ altitude with $0.01 \text{ kg} / \text{m}^2 \text{ s}$ of mass injection. The panels to be cooled are determined by $q_{c,w} (W / \text{m}^2)$	65
4-17.	Flight time v.s. reduction of heat energy (kJ) at $M = 6$ and $30000m$ altitude with $0.01 \text{ kg} / \text{m}^2 \text{ s}$ of mass injection. The panels to be cooled are determined by $q_{c,w} (W / \text{m}^2)$	65
4-18.	Bottom view of X24C with $50000 W / \text{m}^2$ of allowable $q_{c,w}$ at $30000m$ altitude.....	66
4-19.	Side view of X24C with $50000 W / \text{m}^2$ of allowable $q_{c,w}$ at $30000m$ altitude.....	66
4-20.	Top view of X24C with $50000 W / \text{m}^2$ of allowable $q_{c,w}$ at $30000m$ altitude.	66
4-21.	Distribution of panel area with a given heat transfer, $\dot{Q}_{c,w} (W)$ at $M = 6$ and $30000m$ altitude.....	67
4-22.	Distribution of the number of panels with a given heat transfer, $\dot{Q}_{c,w} (W)$ at $M = 6$ and $30000m$ altitude.....	67
4-23.	Mass injection effect on the flight time at $M = 6$ and $30000m$ altitude. The panels to be cooled are determined by $\dot{Q}_{c,w} (W)$	68
4-24.	Mass injection effect on L/D at $M = 6$ and $30000m$ altitude. The panels to be cooled are determined by $\dot{Q}_{c,w} (W)$	68
4-25.	Mass injection effect on reduction of heat power at $M = 6$ and $30000m$ altitude. The panels to be cooled are determined by $\dot{Q}_{c,w} (W)$	69
4-26.	Normalized reduction of heat power v.s. normalized injected mass at $M = 6$ and $30000m$ altitude with $0.001 \text{ kg} / \text{m}^2 \text{ s}$ of mass injection. The panels to be cooled are determined by $\dot{Q}_{c,w} (W)$	69

4-27. Flight time v.s. normalized injected mass at $M = 6$ and $30000m$ altitude with $0.001 \text{ kg/m}^2 \text{ s}$ of mass injection. The panels to be cooled are determined by $\dot{Q}_{c,w}$ (W).....	70
4-28. Flight time v.s. normalized reduction of heat power at $M = 6$ and $30000m$ altitude with $0.001 \text{ kg/m}^2 \text{ s}$ of mass injection. The panels to be cooled are determined by $\dot{Q}_{c,w}$ (W).....	70
4-29. Reduction of heat power (kW) v.s. injected mass rate (kg/s) at $M = 6$ and $30000m$ altitude with $0.001 \text{ kg/m}^2 \text{ s}$ of mass injection. The panels to be cooled are determined by $\dot{Q}_{c,w}$ (W).....	71
4-30. Reduction of heat energy (kJ) v.s. injected mass (kg) at $M = 6$ and $30000m$ altitude with $0.001 \text{ kg/m}^2 \text{ s}$ of mass injection. The panels to be cooled are determined by $\dot{Q}_{c,w}$ (W).....	71
4-31. Flight time v.s. reduction of heat energy (kJ) at $M = 6$ and $30000m$ altitude with $0.001 \text{ kg/m}^2 \text{ s}$ of mass injection. The panels to be cooled are determined by $\dot{Q}_{c,w}$ (W).....	72
4-32. Normalized reduction of heat power v.s. normalized injected mass at $M = 6$ and $30000m$ altitude with $0.01 \text{ kg/m}^2 \text{ s}$ of mass injection. The panels to be cooled are determined by $\dot{Q}_{c,w}$ (W).....	72
4-33. Flight time v.s. normalized injected mass at $M = 6$ and $30000m$ altitude with $0.01 \text{ kg/m}^2 \text{ s}$ of mass injection. The panels to be cooled are determined by $\dot{Q}_{c,w}$ (W).....	73
4-34. Flight time v.s. normalized reduction of heat power at $M = 6$ and $30000m$ altitude with $0.01 \text{ kg/m}^2 \text{ s}$ of mass injection. The panels to be cooled are determined by $\dot{Q}_{c,w}$ (W).....	73
4-35. Reduction of heat power (kW) v.s. injected mass rate (kg/s) at $M = 6$ and $30000m$ altitude with $0.01 \text{ kg/m}^2 \text{ s}$ of mass injection. The panels to be cooled are determined by $\dot{Q}_{c,w}$ (W).....	74
4-36. Reduction of heat energy (kJ) v.s. injected mass (kg) at $M = 6$ and $30000m$ altitude with $0.01 \text{ kg/m}^2 \text{ s}$ of mass injection. The panels to be cooled are determined by $\dot{Q}_{c,w}$ (W).....	74
4-37. Flight time v.s. reduction of heat energy (kJ) at $M = 6$ and $30000m$ altitude with $0.01 \text{ kg/m}^2 \text{ s}$ of mass injection. The panels to be cooled are determined by $\dot{Q}_{c,w}$ (W).....	75

4-38.	Bottom view of X-24C with 40000W of allowable $\dot{Q}_{c,w}$ at $M = 6$ and 30000m altitude.....	75
4-39.	Side view of X-24C with 40000W of allowable $\dot{Q}_{c,w}$ at $M = 6$ and 30000m altitude.....	75
4-40.	Top view of X-24C with 40000W of allowable $\dot{Q}_{c,w}$ at $M = 6$ and 30000m altitude.....	76
4-41.	Distribution of panel area with a given heat transfer, $q_{c,w}$ (W/m^2) at $M = 6$ and 35000m altitude.....	76
4-42.	Distribution of the number of panels with a given heat transfer, $q_{c,w}$ (W/m^2) at $M = 6$ and 35000m altitude.....	76
4-43.	Mass injection effect on the flight time at $M = 6$ and 35000m altitude. The panels to be cooled are determined by $q_{c,w}$ (W/m^2).....	77
4-44.	Mass injection effect on L/D at $M = 6$ and 35000m altitude. The panels to be cooled are determined by $q_{c,w}$ (W/m^2).....	77
4-45.	Mass injection effect on reduction of heat power at $M = 6$ and 35000m altitude. The panels to be cooled are determined by $q_{c,w}$ (W/m^2).....	78
4-46.	Normalized reduction of heat power v.s. normalized injected mass at $M = 6$ and 35000m altitude with 0.001 kg/m^2 s of mass injection. The panels to be cooled are determined by $q_{c,w}$ (W/m^2).....	78
4-47.	Flight time v.s. normalized injected mass at at $M = 6$ and 35000m altitude with 0.001 kg/m^2 s of mass injection. The panels to be cooled are determined by $q_{c,w}$ (W/m^2).....	79
4-48.	Flight time v.s. normalized reduction of heat power at $M = 6$ and 35000m altitude with 0.001 kg/m^2 s of mass injection. The panels to be cooled are determined by $q_{c,w}$ (W/m^2).....	79
4-49.	Reduction of heat power (kW) v.s. injected mass rate (kg/s) at $M = 6$ and 35000m altitude with 0.001 kg/m^2 s of mass injection. The panels to be cooled are determined by $q_{c,w}$ (W/m^2).....	80
4-50.	Reduction of heat energy (kJ) v.s. injected mass (kg) at $M = 6$ and 35000m altitude with 0.001 kg/m^2 s of mass injection. The panels to be cooled are determined by $q_{c,w}$ (W/m^2).....	80

4-51.	Flight time v.s. reduction of heat energy (kJ) at $M = 6$ and $35000m$ altitude with $0.001 \text{ kg} / \text{m}^2 \text{ s}$ of mass injection. The panels to be cooled are determined by $q_{c,w} (W / \text{m}^2)$	81
4-52.	Normalized reduction of heat power v.s. normalized injected mass at $M = 6$ and $35000m$ altitude with $0.01 \text{ kg} / \text{m}^2 \text{ s}$ of mass injection. The panels to be cooled are determined by $q_{c,w} (W / \text{m}^2)$	81
4-53.	Flight time v.s. normalized injected mass at $M = 6$ and $35000m$ altitude with $0.01 \text{ kg} / \text{m}^2 \text{ s}$ of mass injection. The panels to be cooled are determined by $q_{c,w} (W / \text{m}^2)$	82
4-54.	Flight time v.s. normalized reduction of heat power at $M = 6$ and $35000m$ altitude with $0.01 \text{ kg} / \text{m}^2 \text{ s}$ of mass injection. The panels to be cooled are determined by $q_{c,w} (W / \text{m}^2)$	82
4-55.	Reduction of heat power (kW) v.s. injected mass rate (kg / s) at $M = 6$ and $35000m$ altitude with $0.01 \text{ kg} / \text{m}^2 \text{ s}$ of mass injection. The panels to be cooled are determined by $q_{c,w} (W / \text{m}^2)$	83
4-56.	Reduction of heat energy (kJ) v.s. injected mass (kg) at $M = 6$ and $35000m$ altitude with $0.01 \text{ kg} / \text{m}^2 \text{ s}$ of mass injection. The panels to be cooled are determined by $q_{c,w} (W / \text{m}^2)$	83
4-57.	Flight time v.s. reduction of heat energy (kJ) at $M = 6$ and $35000m$ altitude with $0.01 \text{ kg} / \text{m}^2 \text{ s}$ of mass injection. The panels to be cooled are determined by $q_{c,w} (W / \text{m}^2)$	84
4-58.	Bottom view of X-24C with $30000 \text{ W} / \text{m}^2$ of allowable $q_{c,w}$ at $35000m$ altitude.	84
4-59.	Side view of X-24C with $30000 \text{ W} / \text{m}^2$ of allowable $q_{c,w}$ at $35000m$ altitude.	84
4-60.	Top view of X-24C with $30000 \text{ W} / \text{m}^2$ of allowable $q_{c,w}$ at $35000m$ altitude.	85
4-61.	Distribution of panel area with a given heat transfer, $\dot{Q}_{c,w} (W)$ at $M = 6$ and $35000m$ altitude.....	85
4-62.	Distribution of the number of panels with a given heat transfer, $\dot{Q}_{c,w} (W)$ at $M = 6$ and $35000m$ altitude.....	85

4-63.	Mass injection effect on the flight time at $M = 6$ and $35000m$ altitude. The panels to be cooled are determined by $\dot{Q}_{c,w}$ (W).....	86
4-64.	Mass injection effect on L/D at $M = 6$ and $35000m$ altitude. The panels to be cooled are determined by $\dot{Q}_{c,w}$ (W).....	86
4-65.	Mass injection effect on reduction of heat power at $M = 6$ and $35000m$ altitude. The panels to be cooled are determined by $\dot{Q}_{c,w}$ (W).....	87
4-66.	Normalized reduction of heat power v.s. normalized injected mass at $M = 6$ and $35000m$ altitude with $0.001 \text{ kg/m}^2 \text{ s}$ of mass injection. The panels to be cooled are determined by $\dot{Q}_{c,w}$ (W).....	87
4-67.	Flight time v.s. normalized injected mass at $M = 6$ and $35000m$ altitude with $0.001 \text{ kg/m}^2 \text{ s}$ of mass injection. The panels to be cooled are determined by $\dot{Q}_{c,w}$ (W).....	88
4-68.	Flight time v.s. normalized reduction of heat power at $M = 6$ and $35000m$ altitude with $0.001 \text{ kg/m}^2 \text{ s}$ of mass injection. The panels to be cooled are determined by $\dot{Q}_{c,w}$ (W).....	88
4-69.	Reduction of heat power (kW) v.s. injected mass rate (kg/s) at $M = 6$ and $35000m$ altitude with $0.001 \text{ kg/m}^2 \text{ s}$ of mass injection. The panels to be cooled are determined by $\dot{Q}_{c,w}$ (W).....	89
4-70.	Reduction of heat energy (kJ) v.s. injected mass (kg) at $M = 6$ and $35000m$ altitude with $0.001 \text{ kg/m}^2 \text{ s}$ of mass injection. The panels to be cooled are determined by $\dot{Q}_{c,w}$ (W).....	89
4-71.	Flight time v.s. reduction of heat energy (kJ) at $M = 6$ and $35000m$ altitude with $0.001 \text{ kg/m}^2 \text{ s}$ of mass injection. The panels to be cooled are determined by $\dot{Q}_{c,w}$ (W).....	90
4-72.	Normalized reduction of heat power v.s. normalized injected mass at $M = 6$ and $35000m$ altitude with $0.01 \text{ kg/m}^2 \text{ s}$ of mass injection. The panels to be cooled are determined by $\dot{Q}_{c,w}$ (W).....	90
4-73.	Flight time v.s. normalized injected mass at $M = 6$ and $35000m$ altitude with $0.01 \text{ kg/m}^2 \text{ s}$ of mass injection. The panels to be cooled are determined by $\dot{Q}_{c,w}$ (W).....	91

4-74.	Flight time v.s. normalized reduction of heat power at $M = 6$ and $35000m$ altitude with $0.01 \text{ kg} / \text{m}^2 \text{ s}$ of mass injection. The panels to be cooled are determined by $\dot{Q}_{c,w}$ (W).	91
4-75.	Reduction of heat power (kW) v.s. injected mass rate (kg / s) at $M = 6$ and $30000m$ altitude with $0.01 \text{ kg} / \text{m}^2 \text{ s}$ of mass injection. The panels to be cooled are determined by $\dot{Q}_{c,w}$ (W).	92
4-76.	Reduction of heat energy (kJ) v.s. injected mass (kg) at $M = 6$ and $35000m$ altitude with $0.01 \text{ kg} / \text{m}^2 \text{ s}$ of mass injection. The panels to be cooled are determined by $\dot{Q}_{c,w}$ (W).	92
4-77.	Flight time v.s. reduction of heat energy (kJ) at $M = 6$ and $35000m$ altitude with $0.01 \text{ kg} / \text{m}^2 \text{ s}$ of mass injection. The panels to be cooled are determined by $\dot{Q}_{c,w}$ (W).	93
4-78.	Bottom view of X-24C with $20000W$ of allowable $\dot{Q}_{c,w}$ at $35000m$ altitude.	93
4-79.	Side view of X-24C with $20000W$ of allowable $\dot{Q}_{c,w}$ at $35000m$ altitude.	93
4-80.	Top view of X-24C with $20000W$ of allowable $\dot{Q}_{c,w}$ at $35000m$ altitude.	94

Abstract of Thesis Presented to the Graduate School
of the University of Florida in Partial Fulfillment of the
Requirements for the Degree of Master of Science

REDUCING SKIN FRICTION AND HEAT TRANSFER OVER A HYPERSONIC CRUISING
VEHICLE BY MASS INJECTION

By

Yoshifumi Nozaki

August 2007

Chair: Pasquale M. Sforza
Major: Aerospace Engineering

Demonstrating technologies for hypersonic aircraft that cruise at speeds greater than Mach 5 is one of the long-term visions of many agencies, like NASA. Reducing skin friction and heat transfer on the surface of hypersonic cruising vehicles has been a focus of constant attention. General methods for estimating the aerodynamic forces and heat transfer around a hypersonic vehicle are used to evaluate the reduction in skin friction and heat transfer on the surface of a hypersonic vehicle by mass injection. Particular attention was paid to the X-24C configuration because of the existence of experimental data of X-24C performance against which the predictions can be compared. The local surface inclination method and the flat plate reference enthalpy methods for laminar and turbulent flow were used to find aerodynamic forces and heat transfer. High temperature effects were included by using a classical approximation of thermodynamic properties. Although this analysis is based on many approximations, these methods worked well and flow properties were reasonably predicted. Reducing skin friction and protecting surfaces from heating by injecting mass did result in a penalty in the form of decreased flight time of the vehicle, and therefore flight range. These penalties were often very light. Also, as more mass is injected, the effect of mass injection grows, but more slowly.

CHAPTER 1 INVISCID ANALYSIS

Introduction

Hypersonic flow is complicated because of physical aspects of hypersonics such as high-temperature chemically reacting, thin shock layer, etc. Such complex phenomena cannot be described by a simple linear system. Even without these phenomena, the basic theory of inviscid compressible flow, when the Mach number is very large, does not yield aerodynamic theories which are mathematically linear. By using supersonic thin airfoil theory, the pressure coefficient on the surface is obtained from

$$c_p = \frac{2\theta_i}{\sqrt{M_\infty^2 - 1}} \quad (1-1)$$

where M_∞ is the free stream Mach number, and θ_i is flow inclination. Eq.(1-1) is a classical result from inviscid, linearized, two-dimensional, supersonic flow theory.¹ This method is called the local surface inclination method, and it is very simple and easy to use to predict c_p . This method does not need a detailed solution of the complete flowfield. This simplicity is very useful, but unfortunately, it is not valid for hypersonic speeds since nonlinear effects become important at high Mach number. However, there are other valid local surface inclination methods, and some of those are presented, which are applied to our hypersonic bodies.

Local Surface Inclination Method

As M_∞ approaches ∞ and γ approaches 1, the shock layer becomes coincident with the body surface. This is because the density ratio across the shock approaches zero, and since the density behind the shock is so high the shock layer becomes thinner and thinner. Therefore, it looks as if the incoming flow is directly impinging on the wedge surface, and then is running parallel to the surface downstream. Under these conditions, Newtonian theory is used to find c_p .

For blunt bodies the modified Newtonian theory should be used, and such results usually produce acceptable accuracy. In contrast, Anderson² suggests that Newtonian results for slender bodies should use the straight Newtonian theory. Newtonian theory works reasonably well alone and lends itself to application to arbitrary slender body shapes. In the Newtonian model of fluid flow, the particles in the free-stream impact only on the frontal area of the body; they cannot curl around the body and impact on the back surface. Hence, for that portion of a body which is in the “shadow” of the incident flow, no impact pressure is left, so over this “shaded” region the Newtonian theory is inaccurate. Therefore the Newtonian theory is described by the following equations:

$$c_p = 2 \cdot \frac{(\vec{V}_\infty \cdot \hat{n})^2}{\vec{V}_\infty \cdot \vec{V}_\infty} \text{ for } \vec{V}_\infty \cdot \hat{n} < 0 \quad (1-2)$$

$$c_p = 0 \text{ for } \vec{V}_\infty \cdot \hat{n} \geq 0 \quad (1-3)$$

where \hat{n} is unit outward normal vector on the body surface. The above equations are locally applicable to every surface panel on a smooth body. In order to have more accurate results, Prandtl-Meyer expansion theory should be applied for the surface panel at which the Newtonian method is inaccurate. In this study, we use Newtonian theory for all surface panels except for the part in the “shadow”, at which we applied Prandtl-Meyer expansion theory. In practice, the body surface of a vehicle is subdivided into a number of individual panels and each panel is treated separately to determine the pressure force acting. In this study, the surface of the X-24C vehicle is divided into 284 panels as described subsequently. The normal vector of each panel can be found by the cross-product of the P and Q vector as shown in Figure 1-1.

$$\vec{N} = \vec{P} \times \vec{Q} \quad (1-4)$$

$$\hat{n} = \frac{\vec{N}}{\sqrt{\vec{N} \cdot \vec{N}}} \quad (1-5)$$

$$dA = \frac{1}{2} |\vec{P} \times \vec{Q}| = \frac{1}{2} |\vec{N}| \quad (1-6)$$

where dA is differential area of individual panel. Once having the unit normal to the surface element, the pressure force acting on each panel can be found by:

$$d\vec{F}_{press} = -(c_p q + P_\infty) \cdot dA \cdot \hat{n} \quad (1-7)$$

$$q = \frac{1}{2} \rho_\infty V_\infty^2 \quad (1-8)$$

where $d\vec{F}_{press}$ is the pressure force acting on individual panel and q is the dynamic pressure.

Inviscid Aerodynamic Forces and Moments

Before determining differential lift(dL) and drag(dD) on each panel, the angle of attack must be accounted for the flow condition. In this analysis, the angle of attack is defined as the angle between the free stream velocity vector (or x-axis) and the fuselage reference line of the vehicle. Therefore, each node point must be rotated with respect to y-axis as the angle of attack increases (the origin of the coordinate is located at the nose of the vehicle). The following equations are used to change each node on the surface according to variable angle of attacks:

$$x' = \sqrt{x^2 + z^2} \cos\left(\tan^{-1}\left(\frac{z}{x}\right) - \alpha\right) \quad (1-9)$$

$$y' = y \quad (1-10)$$

$$z' = \sqrt{x^2 + z^2} \sin\left(\tan^{-1}\left(\frac{z}{x}\right) - \alpha\right) \quad (1-11)$$

(x, y, z) : a node at $\alpha = 0$

(x', y', z') : a node at nonzero α

Having the differential pressure force acting on each panel with an accounting for the angle of attack, differential lift(dL) and drag(dD) on each panel are found as:

$$dL_{invisc} = dF_{press,z} \quad (1-12)$$

$$dD_{invisc} = dF_{press,x} \quad (1-13)$$

$$d\vec{F} = dF_{press,x} \hat{i} + dF_{press,y} \hat{j} + dF_{press,z} \hat{k} \quad (1-14)$$

$$d\vec{F} = d\vec{P} \quad (1-15)$$

where dL_{invisc} and dD_{invisc} are differential lift and drag caused by only the pressure acting on the vehicle. Note that the free stream is always directed in the positive x-direction, and the vehicle rotates with respect to y-axis and the free stream flow direction never changes even though the angle of attack changes. Therefore, lift (L) and drag (D) are always directed in the z-direction and x-direction, respectively. However, the angle of attack changes the normal vector on each surface since the P and Q vectors of each surface change with angle of attack.

The differential moment of each panel about a reference point, say the center of mass, due to the differential force on a particular body surface element is given by:

$$d\vec{M}_0 = \vec{r} \times d\vec{F}' = [(x'' - x_0)\hat{i} + (y'' - y_0)\hat{j} + (z'' - z_0)\hat{k}] \times d\vec{F}' \quad (1-16)$$

$$d\vec{M}_0 = dl\hat{i} + dm\hat{j} + dn\hat{k} \quad (1-17)$$

(l, m, n) : (rolling moment, pitching moment, yawing moment)

(x_0, y_0, z_0) : reference point at zero angle of attack (e.g. center of gravity)

The vehicle in free flight has three rotational degrees of freedom. Three rotational disturbances must be originated at a reference point of the vehicle. However, the coordinate system is not set to the vehicle body, so a vector transformation is necessary as following:

$$x'' = x_c \cos \alpha - z_c \sin \alpha \quad (1-18)$$

$$y'' = y_c \quad (1-19)$$

$$z'' = x_c \sin \alpha + z_c \cos \alpha \quad (1-20)$$

$$d\vec{F}' = (dF_x \cos \alpha - dF_z \sin \alpha)\hat{i} + dF_y\hat{j} + (dF_z \cos \alpha + dF_x \sin \alpha)\hat{k} \quad (1-21)$$

(x'', y'', z'') : center of each panel in the transformed coordinate system

(x_c, y_c, z_c) : center of each panel computed by Eq.(1-9) – (1-11)

The differential force $d\vec{F}'$ calculated by Eq.(1-21) is used in Eq.(1-16). In order to have more accurate pressure force, Prandtl-Meyer expansion theory should be applied for the surface in the “shadow region,” in which the Newtonian theory is inaccurate. This theory will be discussed in the next chapter since Prandtl-Meyer expansion theory is used to aid in determining thermodynamic properties such as viscosity on the shaded surface.

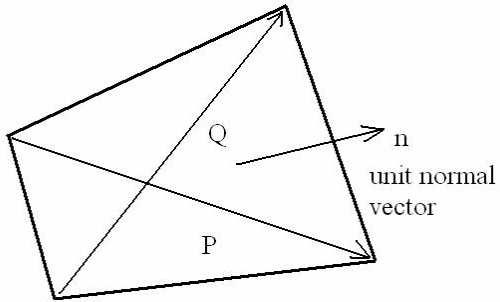


Figure 1-1. General body surface panel showing the unit normal vector along with the locations of the four corner points.

CHAPTER 2 VISCOUS AND HIGH TEMPERATURE CONSIDERATIONS

Introduction

In the preceding analysis the fluid dynamic effects of high Mach number is emphasized, without the added complications of viscous and high temperature effects. However, the matter of friction and thermal conduction should not be neglected since high speed flow is slowed by viscous effects within the boundary layer, and lost kinetic energy is transformed in part into internal energy. This extreme viscous effect can create very high temperatures – high enough to excite vibrational energy within molecules, and to cause dissociation and even ionization within the gas. The geometric layout of the body surface panels, the pressure on each panel, and the determination of the velocity component tangential to the body surface panels all are used in an approximate analysis of the skin friction and heat loads experienced by the vehicle during hypersonic flight. In order to calculate skin friction for both laminar and turbulent flows, the flat plate reference enthalpy method and Reynolds' analogy with heat transfer are used. For very large hypersonic Mach number, the assumption that the pressure is constant in the normal direction through a boundary layer is not always valid. However, for vehicles designed to fly at around $M = 6$ a constant pressure in the normal direction is the case.

Local Reynolds Number

One of the major parameters used in the analysis is the Reynolds number based on the local tangential velocity, temperature, and distance, s , from the stagnation point, that is

$$\text{Re}_{s,e} = \frac{\rho_e \mu_e s}{\mu_e} \quad (2-1)$$

The variable s denotes the distance along the surface of the vehicle measured from the relevant stagnation point or stagnation line, while the subscript e indicates that these variables

are conditions at the outer edge of the boundary layer. The tangential component of the free stream velocity is denoted by u_e , and that is found by the preceding inviscid analysis as

$$\vec{u}_e = \vec{V}_\infty - (\vec{V}_\infty \cdot \hat{n})\hat{n} \quad (2-2)$$

If the x component of the unit vector is positive, and the panel of a body is in the “shadow” of the incident flow, the Prandtl-Meyer expansion relations are applied locally since the Newtonian formula merely has $c_p = 0$ everywhere in the shadow region. Now consider the centered Prandtl-Meyer expansion around a corner of deflection angle θ , as sketched in Figure 2-1. Upstream of the wave is the windward area of a body and the downstream is the shadow area of a body. The Mach numbers upstream and downstream of the wave are M_1 and M_2 , respectively. From basic compressible flow, the relation between θ , M_1 and M_2 is given by:

$$\theta = \nu(M_2) - \nu(M_1) \quad (2-3)$$

where ν is the Prandtl-Meyer function:

$$\nu(M) = \sqrt{\frac{\gamma+1}{\gamma-1}} \tan^{-1} \sqrt{\frac{\gamma-1}{\gamma+1}(M^2-1)} - \tan^{-1} \sqrt{M^2-1} \quad (2-4)$$

From the equation above, the value of ν corresponding to M_1 , and M_2 is found by the tangential components of the free stream velocity u_e at the outer edge of boundary layer. Figure 2-2 shows a 3-dimensional sketch of the flow around the corner. The deflection angle θ is found from the following relation:

$$\theta = \sin^{-1} \frac{u_{e1} \times u_{e2}}{|u_{e1}| |u_{e2}|} = \sin^{-1} (\hat{u}_{e1} \times \hat{u}_{e2}) \quad (2-5)$$

where u_{e1} and u_{e2} are the tangential component of the free stream velocity u_e at the outer edge of boundary layer of upstream and downstream respectively. Both u_{e1} and u_{e2} are found by Eq.(2-2) although u_{e2} obtained by Eq.(2-2) is not real outer edge velocity. In order to find the

deflection angle θ , only the directions of u_{e1} and u_{e2} must be found, so Eq.(2-2) is used only to find the unit vector of u_{e2} . Now θ and M_1 are known, so M_2 can be found by using Eq.(2-3) and Eq.(2-4), and the real u_{e2} and downstream thermodynamic properties are given by:³

$$u_{e2} = M_2 \sqrt{\gamma R_{air} T_2} \quad (2-6)$$

$$T_2 = T_1 \frac{1 + \left(\frac{\gamma-1}{2}\right) M_1^2}{1 + \left(\frac{\gamma-1}{2}\right) M_2^2} \quad (2-7)$$

$$P_2 = P_1 \left(\frac{T_2}{T_1}\right)^{\frac{\gamma}{\gamma-1}} \quad (2-8)$$

$$\rho_2 = \rho_1 \left(\frac{T_2}{T_1}\right)^{\frac{1}{\gamma-1}} \quad (2-9)$$

In order to find the downstream thermodynamic properties, the upstream thermodynamic properties must be known.

For a specific value of γ , the Prandtl-Meyer function ν asymptotically approaches the maximum value ν_{\max} as Mach number increases. Thus, if $\nu(M_2) > \nu_{\max}$, an infinite Mach number is generated and the pressure falls to zero. Expansion at such condition would, according to the pressure theory, lead to a vacuum adjacent to the wall. Of course, in reality, the continuum and ideal gas assumption become invalid long before this situation is reached. However, panels whose ν may be greater than ν_{\max} won't have high heat exchange or skin friction. What we need for this study is identifying those surface panels whose total heat transfer is not negligible, so an accurate analysis for these special cases of large expansion angles is not necessary.

In order to evaluate the density and viscosity, the pressure and temperature are required. Since the pressure is assumed to be constant in the direction normal to the panel, the pressure on

the panels may be obtained from the pressure coefficients obtained in chapter 1 or Eq.(2-8) for the shaded panels, and that is

$$P_w = P_e = c_p q + P_\infty$$

or $P_w = P_e = P_2$ by Eq.(2-8) for shaded panels (2-10)

Temperature may be obtained by using the energy equation along a streamline

$$h_{total} = h_\infty + \frac{1}{2}V_\infty^2 = h_e + \frac{1}{2}u_e^2 \quad (2-11)$$

Therefore,

$$h_e = h_\infty + \frac{1}{2}V_\infty^2 - \frac{1}{2}u_e^2 = C_{p,\infty}T_\infty + \frac{1}{2}V_\infty^2 - \frac{1}{2}u_e^2 \quad (2-12)$$

where $C_{p,\infty}$ is constant pressure specific heat at temperature of T_∞ . The assumption here is that kinetic energy carried in the normal component of velocity is transformed into internal energy by adiabatic compression. In order to find the temperature from enthalpy, it is necessary to use tables or models for the thermodynamic and transport properties of high temperature air. Here Hansen's "Approximations for the Thermodynamic and Transport Properties of High-Temperature Air"⁴ is used to evaluate the behavior of thermodynamic and transport properties at high temperature.

Numerical codes are used to predict temperature, compressibility, density, viscosity, and Prandtl number. Prandtl number is not used to find Reynolds number, but will be used to find skin friction later, so the code computing Prandtl number is introduced here. The code for computing the temperature needs only inputs of enthalpy and pressure which are already known. The other codes computing compressibility, density, viscosity, and Prandtl number need inputs of pressure and temperature which is obtained from the code computing temperature. However, in order to find the temperature from pressure and enthalpy, the compressibility must be known since temperature is defined as a function of enthalpy, pressure, and compressibility in Hansen,

and inversely compressibility is obtained from pressure and temperature. Pressure and enthalpy are known, and therefore the temperature is guessed, and an iteration is carried out until the given enthalpy matches the enthalpy computed from guessed temperature. This approach establishes the following five functions.

$$T = T(P, h) \tag{2-13}$$

$$Z = Z(P, T) \tag{2-14}$$

$$\rho = \rho(P, T) \tag{2-15}$$

$$\mu = \mu(P, T) \tag{2-16}$$

$$\text{Pr} = \text{Pr}(P, T) \tag{2-17}$$

To find the distance s , the stagnation point (stagnation line for the wing) must be specified. Here it is assumed that for typical vehicles, like the X-24C that will be studied in this paper, there is one stagnation point for the fuselage while the two-dimensional cross section of the wings (airfoils) have stagnation lines. We can set the stagnation point at the center of the panel whose outward normal vector is the closest to the opposite vector of free stream. In this study, the vehicle has only low angles of attack, so the stagnation points are always located at the most windward panel. The most windward panel is so small that s of other panels do not change much even if the stagnation point and line are shifted to the nose of the fuselage and leading edge of the wing. Therefore, the stagnation point and line are set to the nose point of the fuselage and leading edge of the wings, respectively for convenience. The distance s is assumed to be the distance from the stagnation point to the center of the panel under consideration.

Local Skin Friction

The Van Driest II method for turbulent boundary layers is probably the most accurate generally applicable equation for skin friction, but it is too complicated for the entire surface of a vehicle. Another simpler method uses a reference value of temperature at which the density and physical properties of the fluid are evaluated and used in the available constant density, constant

property boundary layer solutions to provide an adequate approximation to the actual, variable density, variable property flow. That value of the temperature is called the reference temperature, T^* .⁵ In this study, the flat plate reference enthalpy method is utilized to determine local surface heat transfer and Reynolds' analogy with heat transfer for laminar and turbulent flow is used to determine friction on panels. The flat plate panels considered here have approximately constant pressure over the skin surface, and thus permits this approach. The Nusselt number is given by

$$Nu = A \left(\frac{\rho^*}{\rho_e} \right)^a \left(\frac{\mu^*}{\mu_e} \right)^b \text{Re}_{s,e}^c (\sqrt{3})^j \quad (2-18)$$

The coefficients in Eq.(2-18) are listed in Table 2-1. The reference enthalpy and the adiabatic wall enthalpy are given by

$$h^* = 0.28h_e + 0.5h_w + 0.22h_{aw} \quad (2-19)$$

$$h_{aw} = h_e + \text{Pr}_e^m \frac{u_e^2}{2} \quad (2-20)$$

where h_e and h_w are the enthalpies at the edge of the boundary layer and at the wall, respectively, and Pr_e is the Prandtl number evaluated at the edge of boundary layer. The quantity m is 1/2 for laminar flow and 1/3 for turbulent flow. It is noted that the skin friction coefficient and the Nusselt number are related. This observation can be formalized an generalized for non-slip condition, $u_w = 0$, and the relation is

$$Nu = \text{Re} \cdot \text{Pr}^{\frac{1}{3}} \frac{c_f}{2} \quad (2-21)$$

or

$$c_f(s) = \frac{2A}{\text{Pr}^{1/3}} \left(\frac{\rho^*}{\rho_e} \right)^a \left(\frac{\mu^*}{\mu_e} \right)^b \text{Re}_{s,e}^{c-1} (\sqrt{3})^j \quad (2-22)$$

where $c_f(s)$ is the local skin friction coefficient.

Local Heat Transfer

From Eq.(2-21) and Eq.(2-22), the local heat transfer can be found since the definition of the Nusselt number is

$$Nu = \frac{q_{c,w}s}{k_e(T_w - T_{aw})} \quad (2-23)$$

where $q_{c,w}$ is the convective heat transfer at the wall, and is obtained from the relation

$$q_{c,w} = \frac{c_f(s) Pr_e^{1/3} Re_{s,e} k_e (T_w - T_{aw})}{2s} \quad (2-24)$$

The subscripts w and e denote conditions at the wall and the edge of the boundary layer. Eq.(2-24) provides reasonable values for the heat transfer, except for the extremely high value at the region near the stagnation point, since the distance from the stagnation point, s is very small around the stagnation point. Thus, the blunt body heat transfer method is applied to the region near the stagnation point. Fay and Riddell^{6, a} first carried out a rigorous study of stagnation point convective heat transfer at hypersonic speeds and provided the following result

$$q_{c,s} = 0.76 Pr^{-0.6} (\rho_e \mu_e)^{0.4} (\rho_w \mu_w)^{0.1} \sqrt{\left(\frac{du_e}{ds}\right)_s} (h_{s,e} - h_w) \left[1 - (Le^{0.52} - 1) \left(\frac{h_D}{h_{s,e}}\right) \right] \quad (2-25)$$

In Eq.(2-25), the term in square brackets represents the effects of equilibrium chemical reactions occurring in the stagnation region and

$$Le = \frac{\rho D_{12} c_p}{k} \quad (2-26)$$

$$h_D = \sum_{i=1}^n c_i \Delta h_{f,i} \quad (2-27)$$

The gas considered here is air, which can be considered to be a binary mixture. This mixture is made up of two species: oxygen and nitrogen atoms (O and N) and molecules (O₂ and

^a Taken from "Space Access Vehicle Design Handbook" (Sforza, P. M.)

N2). The quantity D_{12} is the binary diffusion coefficient. The quantities c_i and $\Delta h_{f,i}$ are the molar concentrations of the individual species (O, O₂, N, and N₂) and the chemical heat of formation of each species, respectively. The Lewis number for an air-like mixture given by Eq.(2-26) is close to unity, $Le \sim 1.4$, so that the quantity $(Le^{0.52} - 1) \sim 0.19$, and the contribution of the chemical reaction term can be often be safely neglected.

The velocity gradient at the stagnation point in Eq.(2-25) may be found by

$$\frac{du_e}{ds} = \frac{1}{R_b} \sqrt{\frac{2(P_e - P_\infty)}{\rho_e}} \quad (2-28)$$

In the Newtonian approximation this becomes

$$\frac{du_e}{ds} \approx \sqrt{2\varepsilon} \frac{V_\infty}{R_b} \quad (2-29)$$

Then Eq.(2-25) is simplified to

$$q_{c,s} = \frac{0.9038}{\varepsilon^{1/4}} \left(\frac{C_w}{Pr} \right)^{0.1} \sqrt{\frac{\rho_\infty V_\infty \mu_s}{R_b Pr}} (h_{s,e} - h_w) \quad (2-30)$$

In Eq.(2-30) the variable $C_w = \rho_w \mu_w / \rho_s \mu_s$ is the Chapman-Rubesin factor and the Prandtl number is calculated at the stagnation conditions at the edge of the boundary layer. The stagnation enthalpy behind the shock as well as the density ratio across the shock can be determined from the shock relations for equilibrium air chemistry. A schematic diagram of stagnation region is shown in Figure 2-3.

A stationary normal shock wave is considered here. The shock is so strong that the temperature behind the shock is high enough to ensure that vibrational excitation and chemical reactions occur behind the shock front. It is assumed that local thermodynamic and chemical equilibrium conditions hold behind the shock, and all conditions ahead of the shock wave are known. The governing equations for the flow across a normal shock are

$$\text{Continuity } \rho_1 u_1 = \rho_2 u_2 \quad (2-31)$$

$$\text{Momentum } P_2 = P_1 + \rho_1 u_1^2 \left(1 - \frac{\rho_1}{\rho_2}\right) \quad (2-32)$$

$$\text{Energy } h_2 = h_1 + \frac{u_1^2}{2} \left[1 - \left(\frac{\rho_1}{\rho_2}\right)^2\right] \quad (2-33)$$

In addition, the equilibrium thermodynamic properties for the high-temperature gas are known from the numerical techniques introduced by Eq. (2-13) and Eq.(2-15). The codes used here are

$$T_2 = T(P_2, h_2) \quad (2-34)$$

$$\rho_2 = \rho(P_2, T_2) \quad (2-35)$$

Since all the upstream conditions, ρ_1 , u_1 , P_1 , h_1 , etc., are known, Eq.(2-32) and Eq.(2-33) express P_2 and h_2 , respectively, in terms of only one unknown ρ_1/ρ_2 . This establishes the basis for an iterative numerical solutions introduced by Anderson², as follows

1. Assume a value for ρ_1/ρ_2 . (A value of 0.1 is usually good first guess.)
2. Compute P_2 from Eq.(2-32) and h_2 from Eq.(2-33)
3. Using the values of P_2 and h_2 obtained, compute T_2 from Eq.(2-34) and ρ_2 from Eq.(2-35).
4. Form a new value of ρ_1/ρ_2 from the value of ρ_2 obtained in step 3.
5. Use this new value of ρ_1/ρ_2 in Eq.(2-32) and Eq.(2-33) to obtain new values of P_2 and h_2 , respectively. Then repeat step 2 through 5 until convergence is obtained, i.e., until there is only a negligible change in ρ_1/ρ_2 from one iteration to the next.
6. At this stage, the correct values of P_2 , h_2 , T_2 , and ρ_2 are obtained. Using Eq.(2-31), obtain the correct value of u_2 .

By means of step 1 through 6 above, all properties behind the shock wave are found for given properties in front of the wave.

